Available online at www.sciencedirect.com

SciVerse ScienceDirect

Ceramics International 39 (2013) 571–578

CERAMICS INTERNATIONAL

www.elsevier.com/locate/ceramint

SiO_2–Al_2O_3–CaO glass-ceramics: Effects of CaF_2 on crystallization, microstructure and properties

Debasis Pradip Mukherjee, Sudip Kumar Das*

Department of Chemical Engineering, University of Calcutta, 92, A P C Road, Kolkata-700009, India

Received 14 May 2012; received in revised form 20 June 2012; accepted 20 June 2012
Available online 5 July 2012

Abstract

The effects of fluorine content on the nucleation and crystallization behavior of SiO_2–Al_2O_3–CaO glass ceramics system have been investigated. The crystalline phases were determined by X-ray diffraction (XRD). The crystallization kinetics was determined by differential thermal analysis (DTA). The microstructures were examined by using scanning electron microscope (SEM). Fourier transformed infrared spectra (FTIR) analysis was used to study the glass structure. The results showed that by increasing the fluorine content, both the crystallization peak temperature (T_p) and activation energy (E) decreased. Wollastonite, anorthite and gehlenite are the main crystalline phases that exist in the glass ceramics system. The study shows that fluorine promoted initial crystallization of glass and can be used as an effective nucleating agent in the SiO_2–Al_2O_3–CaO system.

Keywords: D. Glass ceramics; Crystallization; FTIR; SEM

1. Introduction

Glass ceramics materials are polycrystalline solids, prepared by the controlled crystallization technique. Glass ceramics are used for clinical purpose, but their low toughness properties have limited their use to only non-load bearing applications [1–3]. However, their properties depend on the composition of phases and microstructure developed during the manufacturing process. The basic glassy components present in these materials are SiO_2–Al_2O_3–CaO and nucleating agents are required for proper nucleation and crystallization. Literature review suggested that the wide varieties of chemicals like, TiO_2, CaF_2, ZrO_2, P_2O_5, Cr_2O_3, Fe_2O_3, V_2O_5, MoO_3 can be used as nucleating agents. The use of TiO_2 as nucleating agent encouraged the phase separation and also formation of many nucleating sites in LAS (LiO_2–Al_2O_3–SiO_2) [4]. Barry et al. [5] observed that the use of TiO_2 as nucleating agent decreased the surface tension and increased the rate of nucleating in LAS. The use of ZrO_2 as nucleating agent improved mechanical properties, particularly the fracture toughness and wear resistance [6,7]. Liu and Chen [8] reported that ZrO_2 did not induce bulk crystallization process in K_2O–MgO–Al_2O_3–SiO_2 system. The addition of P_2O_5 as a nucleating agent in SiO_2–LiO_2–K_2O–ZnO–P_2O_5 glass system promoted bulk nucleation and produced an interlocking morphology with very fine grains [9]. Guedes et al. [10] used TiO_2 and ZrO_2 as nucleating agents and reported their effect on the crystalline phases, transition temperature and the texture of the LAS. Additions of different nucleating agents like CaF_2, LiF and TiO_2 in Na_2O–CaO–MgO–Al_2O_3-SiO_2 glass system were studied by Salama et al. [11] and they concluded that the fluorine facilitated the formation of aluminosilicates and CaF_2 addition produced fine-grained microstructures as compared to LiF. Guseva and Gulyukin [12] studied the effects of different fluorine addition on the SiO_2–CaO–Al_2O_3 glass system and concluded that CaF_2 containing samples possessed the densest crystalline structure. The use of MgF_2 as a nucleating agent in LAS system showed that the fluorine promoted initial crystallization

*Corresponding author. Tel.: +91 9830638908.
E-mail address: drsudipkdas@vsnl.net (S.K. Das).

0272-8842/$36.00
http://dx.doi.org/10.1016/j.ceramint.2012.06.066

and diffusion in the glass system [13]. Combined effects of different nucleating agents like Cr_2O_3, Fe_2O_3 and TiO_2 on the cryatallization behavior of SiO_2–Al_2O_3–CaO–MgO glass system were reported by Rezvani et al. [14]. Li-ping and Hanining [15] reported the use of P_2O_5 as a nucleating agent in SiO_2–Al_2O_3–ZrO_2 glass system and showed that the main crystalline phases were spinel, anorthite and tetragonal zirconia and the binding strength of the crystals were found to be 120 MPa. The effects of different nucleating agents (TiO_2, Cr_2O_3 and ZrO_2) on the glass system LiO_2–Al_2O_3–SiO_2 were reported by Al-Harbi [16]. They observed that the use of TiO_2 and Cr_2O_3 a near homogeneous glass ceramic was obtained whereas ZrO_2 produced rod like and round crystals of ceramised glass. They also observed that the coefficient of thermal expansion depended on the type of nucleating agents used. The present paper deals with the effects of CaF_2 as nucleating agent in the SiO_2–Al_2O_3–CaO glass system with respect to their crystalline behavior and properties.

2. Experimental

2.1. Materials and methods

Raw materials used were analytical grade calcium carbonate ($CaCO_3$), alumina (Al_2O_3), silica (SiO_2), and calcium fluoride (CaF_2). All the raw materials were supplied by M/S Merck Specialties Private Limited, India. The ceramised glass samples were prepared by the melt quench technique. Table 1 shows the chemical composition of the different glass batches. In the glass batch the chemicals were weighed by using electronic balance and then mixed in a pestle mortal. The mixed powder samples were placed in recrystallized alumina crucible and melted in an electrically heated furnace. The powdered samples were initially kept at 800 °C for 1 h. for calcination and also for release of water from the starting materials and then reheated to 1450 °C and kept at this temperature for 1 h to form a homogeneous mixture. Molten glasses were then poured into cold water to obtain glass frits. The glass frits were dried and milled to different grain sizes for further study.

The glass powders were mixed with 0.2 wt% carboxy methyl cellulose as a binder and pressed by using a laboratory uniaxial hydraulic press at a pressure of 60 MPa to obtained $50 \times 5 \times 4\,mm^3$ bars and 10 mm diameter pellets. The bars and pellets were then heat treated at a rate of 5 °C/min at temperatures from 800 °C to 1200 °C and soaked for 1 h at the maximum temperature followed by natural cooling to room temperature.

Table 1
Chemical composition of raw materials (g).

Batches	$CaCO_3$	Al_2O_3	SiO_2	CaF_2
BFI	24	43	33	12
BFII	24	43	33	9
BFIII	24	43	33	6

2.2. Characterization techniques

2.2.1. Differential thermal analysis (DTA)

The thermal behavior of the glass batches were monitored by differential thermal analyzer (Pyris Diamond TG/DTA, PerkinElmer, Singapore) in nitrogen atmosphere (150 ml/min) at constant heating rate with α-Al_2O_3 powder as reference material. The glass frits were crushed and sieved through a 325 mesh (< 45 μm) to obtain glass powder for thermal analysis. 20 mg of glass samples were taken in platinum crucible and heated at the rate of 5, 10, 15 and 20 °C/min. to study the kinetics of crystallization and also to calculate the activation energy using the Kissinger equation and Avrami parameter using Augis–Bennett equation.

2.2.2. Fourier transformed infrared spectra (FTIR)

The FTIR analysis (Fourier transform infrared absorption spectra) of the crystallized glass batches were carried out in the range 4000–400 cm^{-1} using a Fourier transform infrared spectrometer (Alpha FTIR, Bruker, Germany). The crystallized glass-ceramics batches were ground to fine powder, and then mixed with powdered KBr as binder, to prepare homogeneous discs for FTIR studies.

2.2.3. X-ray power diffraction (XRD)

XRD analysis was used to identify the crystalline phases present in the crystallized glass batches. The analysis was carried out in Philips powder diffractometer (PANalytical PW3040/60, The Netherlands) using Ni filtered CuKα X-rays with a scanning speed of 1°/min. The XRD pattern was recorded within Bragg angle from 5° to 80° 2θ range. The obtained phases were identified by JCPDS numbers (ICDD-PDF2 data base).

2.2.4. Scanning electron microscopy (SEM)

The SEM (FEI-QUANTA-200) analysis was used to identify the microstructure of the crystallized glass batches. Prior to SEM analysis, glass surfaces were first polished and then chemically etched using 10% HF solution for 15–20 s and then rinsed with water and sonicated to remove any debris.

2.2.5. Density and chemical resistance

The densities of ceramised glasses were measured via Archimedes's method. The chemical resistance was estimated by immersing the rectangular glass ceramic specimens in 50 ml of 1 vol% H_2SO_4 solution and reheated at 100 °C for 1 hr.

3. Results and discussion

3.1. DTA analysis results

The DTA curves of the glass specimens are presented in Fig. 1. Table 2 shows the glass transition temperature, T_g and crystallization peak temperature, T_p. As the fluorine content increased crystallization peak temperature decreased, which is due to the decrease in the melt viscosity and formation of crystalline phases like wollastonite, anorthite and gehlenite [17]. Fluorine facilitates the crystallization process formed through weakened structural glass bonds and hence viscosity decreased [11,13,18]. The F^- ions remained in the dissolved state in the residual glass phase and it does not contribute in the crystalline phase formation. The kinetics of glass crystallization can be described from the Johnson-Mehl-Avrami (JMA) equation [19,20].

$$x = 1 - exp[-(kt)^n] \quad (1)$$

where x is the volume fraction, k is the reaction rate constant and n is the Avrami exponent. The activation energy (E) of the crystallization was obtained from the relationship between the heating rate and the maximum (T_p) in the exothermic peak in the DTA curve. The non-isothermal crystallization kinetics of glass batches can be described by the Kissinger expression [21,22] as

$$\ln\frac{T_p^2}{\beta} = \frac{E}{RT_p} + \ln\frac{E}{Rv} \quad (2)$$

In the above equation T_p is the crystallization peak temperature of the DTA curve β is the heating rate, R is the gas constant, and v is the pre-exponential factor. Table 3 showed the T_p values of the three batches at different heating rates. Fig. 2 shows the variation of $\ln(T_p^2/\beta)$ vs. $1/T_p$ is a linear in nature with the intercepts $\ln(E/Rv)$ and slopes E/R. The values of the E, v and n are shown in Table 4. From the value of activation energy E, the Avrami parameter (n) can be calculated by using the

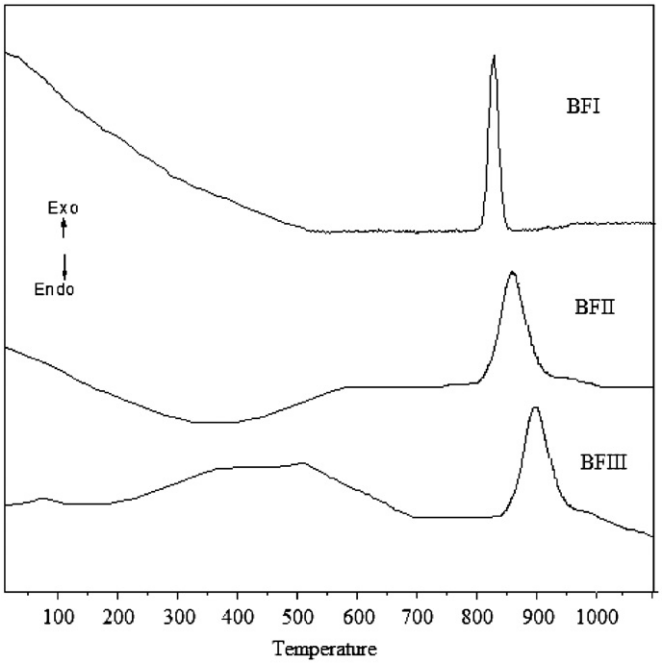

Fig. 1. DTA curves of the different batches at a heating rate at 10 °C/min.

Table 2
Glass transition (T_g) and crystallization peak temperature (T_p).

Batches	T_g (°C)	T_p (°C)
BFI	523	825
BFII	591	867
BFIII	698	893

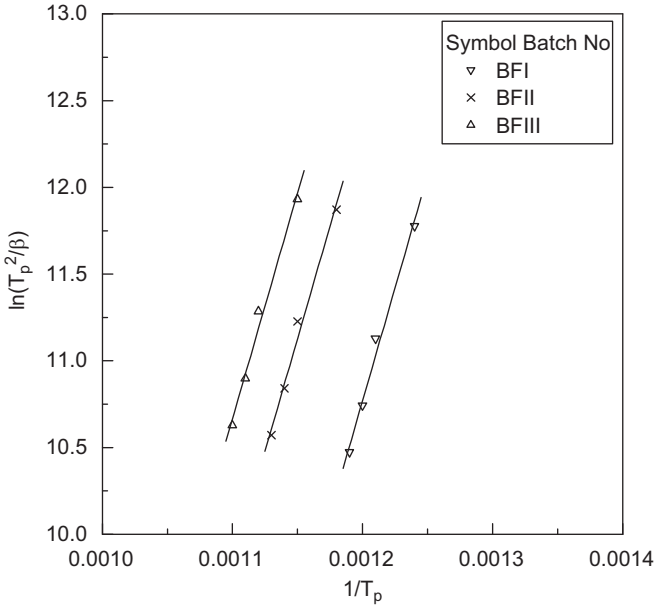

Fig. 2. Variation of $\ln(T_p^2/\beta)$ vs. $1/T_p$ for different glass batches.

Table 3
Crystallization peak temperature (T_p) from DTA results.

	Heating rate			
Batch	5 (K min^{-1}) °C	10 (K min^{-1}) °C	15 (K min^{-1}) °C	20 (K min^{-1}) °C
BFI	807	825	833	841
BFII	847	867	875	883
BFIII	872	893	901	909

Table 4
Activation energy, pre-exponential factor and Avrami parameters values of the samples.

Batch	Activation energy E kJ/mol	Pre-exponential factor v min^{-1}	Avrami parameters (n)
BFI	218.78	2.87×10^{13}	3.23
BFII	218.94	5.89×10^{12}	3.75
BFIII	232.82	1.58×10^{13}	3.96

Table 5
Avrami parameters (n) for different crystallization mechanism.

Mechanism-bulk nucleation	Avrami parameters (n)
Surface crystallization	1
One-dimensional crystal growth	2
Two-dimensional crystal growth	3
Three-dimensional crystal growth	4

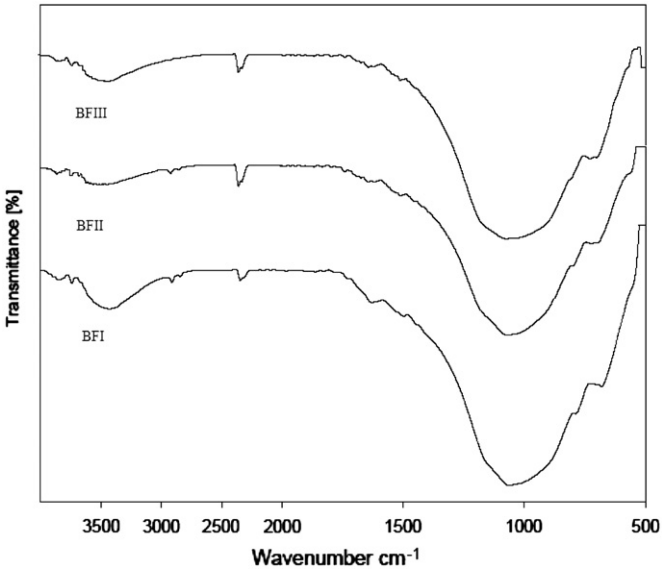

Fig. 3. FTIR spectra of glass batches before heat treatment.

Augis–Bennett equation [23].

$$n = 2.5\frac{RT_p^2}{\Delta TE} \quad (3)$$

where, ΔT is the full width of the exothermic peak at the half maximum intensity from DTA crystallization peak. The value of the Avrami parameter (n) is related to the crystallization mechanism. Table 5 shows the Avrami parameter, n, and its significance in the mechanism of nucleation and crystal growth [24–26]. In the present case the crystal growths are three dimensional homogeneous in nature.

3.2. FTIR analysis results

Figs. 3 and 4 illustrate the FTIR spectra of the sample of glass and heat treated glass samples for all batches. The peak was observed at 3424 cm^{-1} which may be due

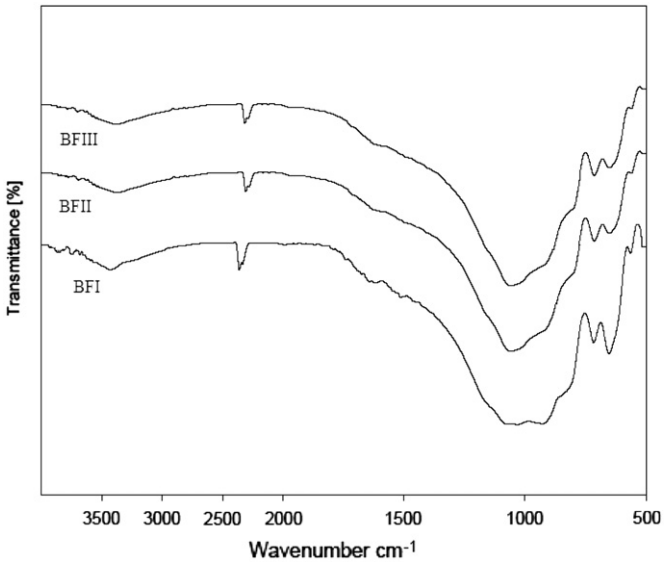

Fig. 4. FTIR spectra of glass batches after heat treatment at 1200 °C for 1 h soaked.

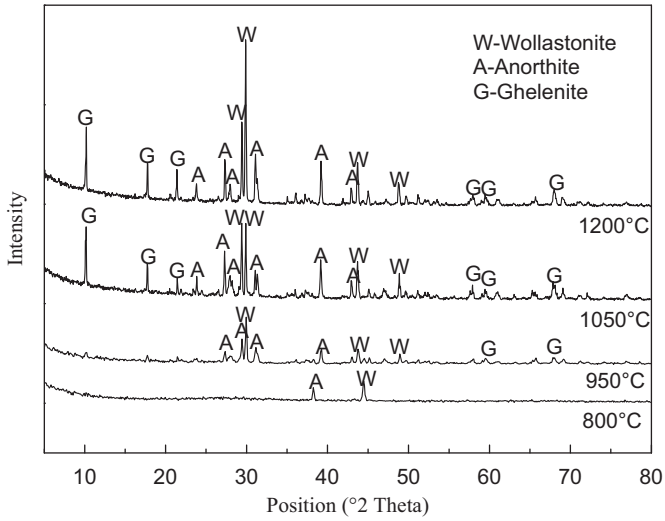

Fig. 5. X-ray diffraction patterns of the batch BFI after heat treated at different temperature.

to the O–H stretching of the surface water and the peak at 1638 cm^{-1} may be due to the vibration of O–H bond or due to the bending of the surface O–H group. Similar observations are reported in the literature [27]. Calcium ions and aluminum Si–O bonds form the bands in the 850 cm^{-1} to 1200 cm^{-1} region. The low energy side of this region is most likely due to Si(OAl/Ca)$_3$ and Si(OAl/Ca)$_4$. The band observed near 930 cm^{-1} is attributed to the stretching vibration of the Si–O bond in the Si(OAl/Ca)$_2$ group. The Si(OAl/Ca)$_2$ group is a silicon–oxygen tetrahedral that has two corners shared with aluminum–oxygen or calcium–oxygen polyhedral [28,29]. 1030–1080 cm^{-1} is attributed to the vibration of the Si(OAl/Ca) group. The vibration of this Si(OAl/Ca) group is the stretching vibration of the silicon–oxygen bond of the SiO_4 tetrahedral with one

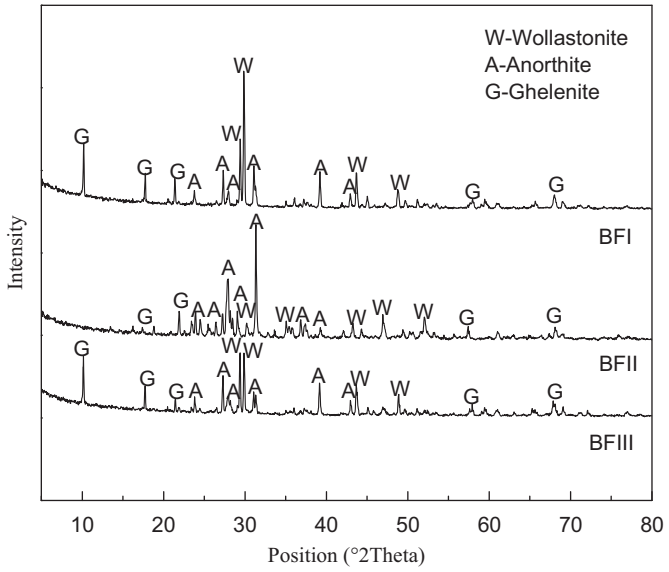

Fig. 6. X-ray diffraction patterns of the glass batches after heat treatment at 1200 °C for 1 h soaked.

Table 6
Crystalline phases identified by XRD analysis.

Sample	Crystalline phases
BFI	$CaSiO_3$, Ca ($Al_2Si_2O_8$), $2CaO.Al_2O_3.SiO_2$
BFII	$CaSiO_3$, Ca ($Al_2Si_2O_8$), $2CaO.Al_2O_3.SiO_2$
BFIII	$CaSiO_3$, Ca ($Al_2Si_2O_8$), $2CaO.Al_2O_3.SiO_2$

Table 7
Analysis of Lattice Deformation from XRD data.

Compositions Main phase	Standard 2θ (deg)	Measured 2θ (deg)	Δ(2θ) (deg)	FWHM (deg)	Deformation (%)
BFI $CaSiO_3$	31.47	31.32	0.15	0.162	0.26
	27.98	27.90	0.08	0.194	0.16
	29.34	29.29	0.05	0.129	0.09
BFII $CaSiO_3$	31.47	31.08	0.39	0.129	0.69
	27.98	27.97	0.01	0.129	0.02
	29.34	29.11	0.23	0.162	0.43
BFIII $CaSiO_3$	31.47	31.34	0.13	0.129	0.23
	27.98	27.92	0.06	0.162	0.12
	29.34	29.05	0.29	0.097	0.55

corner shared with an aluminum or calcium polyhedral [29]. The presence of wollastonite in the glass ceramics is indicated by the spectra of 1060 cm^{-1}, 560 cm^{-1} [30]. The FT-IR peaks at (1030–1070 cm^{-1}) are assigned to the asymmetric stretching vibration of the tetrahedral silicate network. The absorption peak at 930 cm^{-1} is assigned to the $Si–O^-$ stretching vibration with non bridging oxygen. The bands at (800–600 cm^{-1}) are assigned to the Si–O–Si

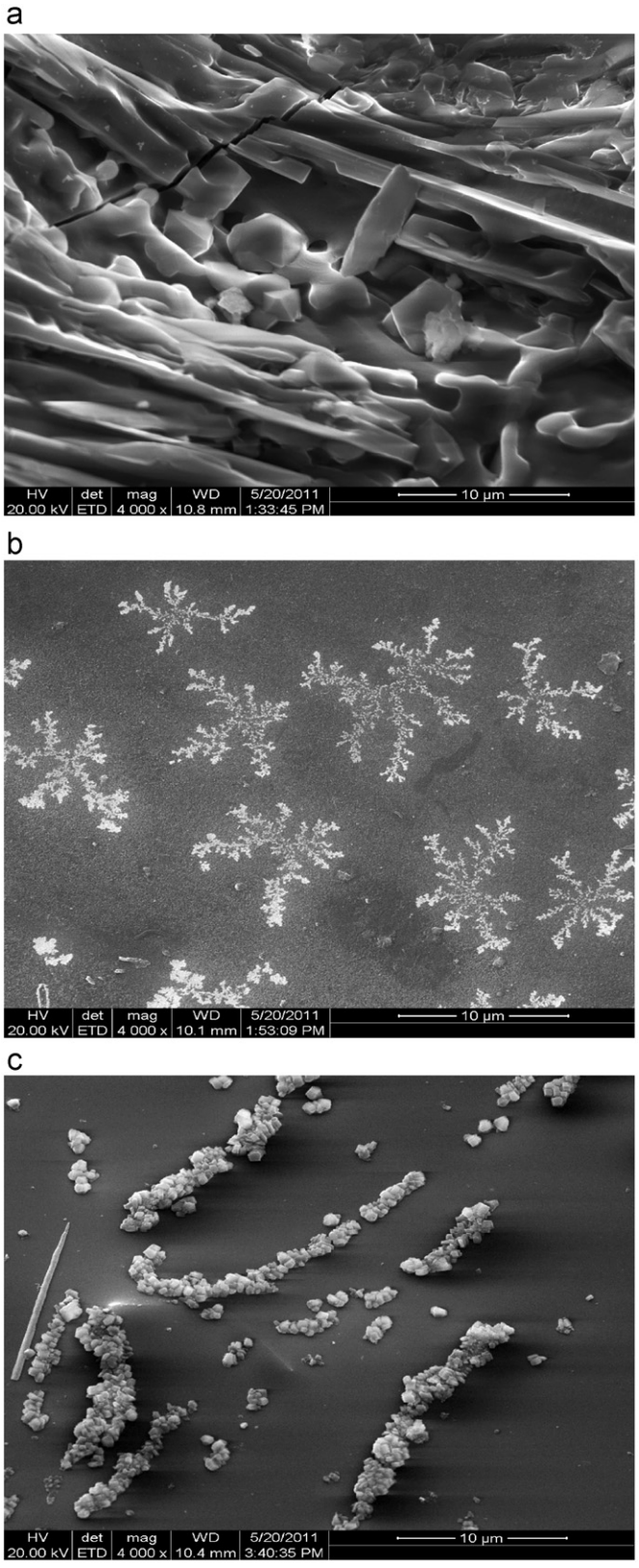

Fig. 7. (a)–(c) SEM micrograph for glass batches after heat treatment at 1200 °C for 1 h soaked (a) BFI, (b) BFII and (c) BFIII.

symmetric stretching vibration of tetrahedral bridging oxygen [31]. The peaks at 650 cm^{-1} and 648 cm^{-1} are assigned to the spectrum of the sample with the presence of CaF_2

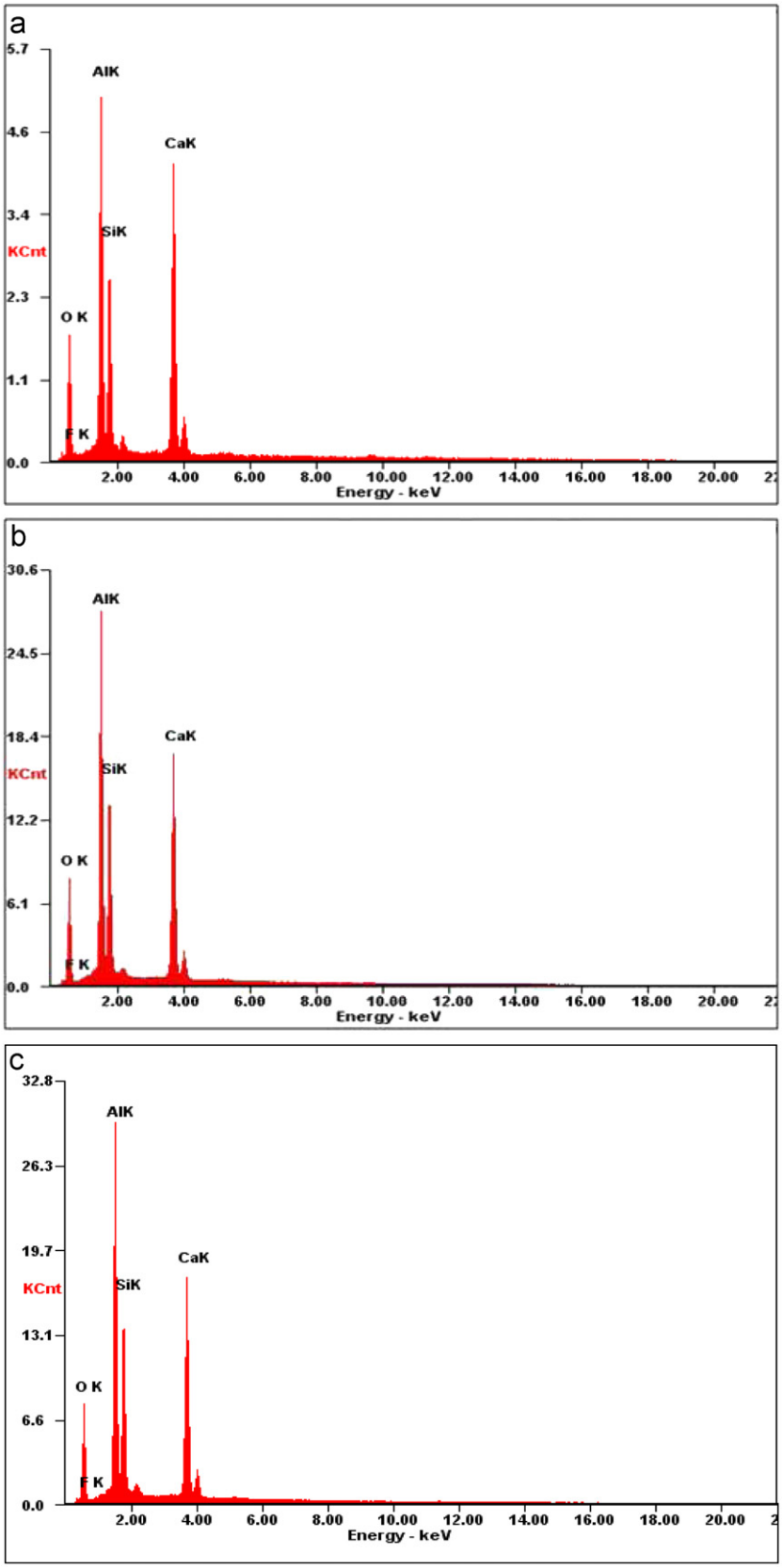

Fig. 8. (a)–(c) EDAX spectrum for glass batches after heat treatment at 1200 °C for 1 h soaked (a) BFI, (b) BFII and (c) BFIII.

components of wollastonite [30]. After heat treatment of the sample, the peaks were observed at 716 cm^{-1} and 650 cm^{-1}, and it might correspond to the bending vibration of Al–O bonds, with Al^{+3} ions in the four-fold coordination (AlO_4). The peak at wave number 560 cm^{-1} is due to the octahedral AlO_6 vibration [32,33].

3.3. XRD analysis results

Fig. 5 shows the X-ray diffraction patterns of the BFI after heat treatment at 800–1200 °C after 1 h soaked. It was found that at 800 °C of the BFI sample is fully amorphous as the peaks are not visible clearly. After heat treatment at 950 °C the results showed formation of wollastonite, anorthite and gehlenite crystal phases. Fig. 6 shows the XRD diagram of all the three batches, BFI, BFII, and BFIII after heat treatment at 1200 °C for 1 h soaked. It is clear from the figure that as the heat treatment temperature increased from 950 °C to 1200 °C the peak intensity increased, which indicated better crystallization. Table 6 shows that the main crystal phases are wollastonite, anorthite and gehlenite which were precipitated during the heat treatment process.

The lattice deformation has been analyzed for different amounts of nucleating agent, i.e., CaF_2 addition using full width at half maximum (FWHM) and the deviations $\Delta(2\theta)$ of the peak position for $CaSiO_3$ phase from the XRD data and is calculated by using the following equation [34]:

$$\varepsilon(\Psi\varphi) = \frac{\Delta(2\theta)(\Psi\varphi)}{2\tan(\theta_0)} \quad (4)$$

where $\varepsilon(\Psi\varphi)$ is the deformation of the corresponding planes, $\Delta(2\theta)$ represents the deviations of peak position, and θ_0 is the standard diffraction angle respectively. The deformation of the lattice in different planes were calculated and shown in Table 7. The full-widths of half maximum approximately varied from 0.194° to 0.097°, which indicated that the sizes of crystals in the glass ceramics for the samples, BFI to BFIII, decreased slightly with increasing CaF_2 content. The deviation range of peak positions for the corresponding glass-ceramics varied from 0.05° to 0.15°, 0.01° to 0.39°, 0.06° to 0.29° for BFI, BFII and BFIII respectively. It showed that the deformation came from the mismatch between the coefficient of thermal expansion of the glass and that of the crystalline phase, and a larger deformation indicates that the crystals are subjected to a greater stress.

3.4. Scanning electron microscopy results

The microstructure of the glass batches prepared after heat-treatment is shown in Fig. 7(a)–(c). Low temperature heat treatment and higher fluorine containing glass samples showed needle like crystal structures distributed around the glass surface and also surface cracks. Similar results were reported by other researchers [17,35]. As CaF_2 amount decreased and heat treatment temperature increased the inter-stars phases of wollastinite (Fig. 7(b)) grew and interlocked with each other. For BFIII glass the chain like lines consisted of small white spheres distributed around the glass was observed. Fig. 8(a)–(c) shows the EDAX analysis. The highest peak belongs to Al and Ca in the EDAX analysis, the wollastonite, anorthite and gehlenite crystalline phases were present in all the batches.

Table 8
Physical and chemical properties of heat treated glass ceramics.

Properties	BFI	BFII	BFIII
Density (gm/cm^3)	2.97	3.03	3.07
Weight loss (%)	2.37	2.23	2.15

3.5. Physical and chemical properties

The density of all the three batches of glass ceramics prepared are reported in Table 8. It is evident from the table that as the amount of fluorine content increases the density decreases but density increases with the increase in heat treatment temperature. The decrease in density may be due to the decomposition of wollastonite and also propagation of surface cracks during the process of crystal growth as observed in SEM. Table 8 shows the chemical resistance of the fully heat treated glass ceramics, i.e., percentage of weight loss in H_2SO_4 test. The results showed that as the fluorine content increases the weight loss for H_2SO_4 solution increased and this loss is due to chemical reaction. The whiteness of glass structure increases with increasing the F^- amount in the glass. The glass ceramics prepared is best suited for floor tile application.

4. Conclusions

Glass ceramics were prepared from SiO_2–Al_2O_3–CaO glass system using different amounts of CaF_2 as nucleating agent and different heat treatment schedules. The addition of CaF_2 into the glass system showed improvement in the microstructure and crystallization properties. The glass crystallization peak temperature (T_p) shifted to lower temperatures as the amount of fluorine increases. The FTIR and XRD indicated that the main crystalline phases were wollastonite, anorthite, gehlenite. The activation energies and avrami parameters calculated from the Johnson-Mehl-Avrami, Kissenger and Augis–Bennett equation for different glass batches (BFI, BFII and BFIII) were formed to be 218.78, 218.94, 232.82 kJ/mol and 3.23, 3.75, 3.96 respectively. These results revealed that the crystals formed were largely homogeneous and three dimensional in nature.

Acknowledgments

The authors would like to thank the UPE scheme of University Grants Commission, University of Calcutta for the financial support.

References

[1] F.H. Lin, M.H. Hon, A study on bioglass ceramics in the Na_2O–CaO–SiO_2–P_2O_5 system, Journal of Materials Science 23 (12) (1988) 4295–4299.

[2] I.D. Thompson, L.L. Hench, Mechanical properties of bioactive glasses, glass-ceramics and composites, Proceedings of the Institution of Mechanical Engineers Part H: Journal of Engineering in Medicine 212 (2) (1998) 127–136.

[3] B. Mirhadia, B. Mehdikhanib, Investigation of crystallization and microstructure of Na_2O–CaO–P_2O_5–SiO_2–Al_2O_3 bio glass ceramic system, New Journal of Glass and Ceramics 2 (2012) 1–6.

[4] P.E. Doherty, D.W. Lee, R.S. Davis, Direct observation of crystallization of Li_2O–Al_2O_3–SiO_2 glasses containing TiO_2, Journal of the American Ceramic Society 50 (2) (1967) 77–81.

[5] T.I. Barry, D. Clinton, L.A. Lay, R.A. Mercer, R.P. Miller, The crystallization of glasses based on eutectic compositions in the system Li_2O–Al_2O_3–SiO_2, Journal of Materials Science 5 (2) (1970) 117–126.

[6] W.M. Chen, K. Chen, Z.D. Deng, Toughening effect of ZrO_2 in glass-ceramics, Journal of Materials Science and Engineering: A 16 (3) (1998) 73–76.

[7] K.G. Chen, J.L. Wan, K.M. Liang, Fabrication of ZrO_2 toughened glass-ceramics, Journal of the Chinese Ceramic Society 26 (3) (1998) 365–368.

[8] L. Ping, C. Xian-Qiu, Phase separation and nucleation in K_2O–MgO–Al_2O_3–SiO_2 glass, Journal of Inorganic Materials 14 (2) (1999) 275–279.

[9] Sascha Cramer von Clausbruch, M. Schweiger, W. Höland, V. Rheinberger, The effect of P_2O_5 on the crystallization and microstructure of glass-ceramics in the SiO_2–LiO_2–K_2O–ZnO–P_2O_5 system, Journal of Non-Crystalline Solids 263–264 (2000) 388–394.

[10] M. Guedes, A.C. Ferro, J.M.F. Ferreira, Nucleation and crystal growth in commercial LAS compositions, Journal of the European Ceramic Society 21 (2001) 1187–1194.

[11] S.N. Salama, S.M. Salama, H. Darwish, The effect of nucleation catalysts on crystallization characteristics of aluminosilicate glasses, Ceram-Silicaty 46 (2002) 15–23.

[12] E.Y. Guseva, M.N. Gulyukin, Effect of fluoride additives on Glass Formation in the SiO_2–CaO–Al_2O_3 system, Inorganic Materials 38 (9) (2002) 962–965.

[13] H. An-Min, L. Kai-Ming, P. Fei, W. Guo-Liang, S. Hua, Crystallization and microstructure changes in fluorine-containing Li_2O–Al_2O_3–SiO_2 glasses, Thermochimica Acta 413 (2004) 53–55.

[14] M. Rezvani, B. Eftekhari-Yekta, M. Solati-Hashjin, V.K. Marghussian, Effect of Cr_2O_3, Fe_2O_3 and TiO_2 nucleants on the crystallization behavior of SiO_2–Al_2O_3–CaO–MgO(R_2O) glass-ceramics, Ceramics International 31 (2005) 75–80.

[15] Y. Li-ping, X. Hanining, H. Peng-fei, Effect of nucleating agents on microstructure and mechanical properties of SiO_2–Al_2O_3–ZrO_2 glass-ceramics, Journal of Central South University of Technology 12 (5) (2005) 507–510.

[16] O.A. Al-Harbi, Effect of different nucleation catalysts on the crystallization of Li_2O–ZnO–MgO–Al_2O_3–SiO_2 glasses, Ceramics International 35 (2009) 1121–1128.

[17] S. Banijamali, B. Eftekhari Yekta, H.R. Rezaie, V.K. Marghussian, Crystalization and sintering characteristics of CaO–Al_2O_3–SiO_2 glasses in the presence of TiO_2, $CaF_2$and ZrO2, Thermochimica Acta 488 (2009) 60–65.

[18] J.A. Griggs, K.J. Anusavice, J.J. Mecholsky, Devitrification and microstructural coarsening of a fluoride-containing barium aluminosilicate glass, Journal of Materials Science 37 (2002) 2017–2022.

[19] M. Avrami, Kinetics of phase change.1. General theory, Journal of Chemical Physics 7 (1939) 1103–1112.

[20] W.A. Johnson, K.F. Mehl, Reaction kinetics in processes of nucleation and growth, Transactions AIME 135 (1939) 416–442.

[21] H.E. Kissinger, Variation of peak temperature with heating rates in differential thermal analysis, Journal of Research of the National Institute of Standards 57 (1956) 217–221.

[22] H.E. Kissinger, Reaction kinetics in differential thermal analysis, Analytical Chemistry 29 (1957) 1702–1706.

[23] J.A. Augis, J.E. Bennett, Calculation of the Avrami parameters for heterogeneous solid state reactions using a modification of the Kissinger method, Journal of Thermal Analysis 13 (1978) 283–292.

[24] K. Cheng, Evaluation of crystallization kinetics of glasses by non-isothermal analysis, Journal of Materials Science 36 (2001) 1043–1048.

[25] L.A. Pérez-Maqueda, J.M. Criado, J. Málek, Combined kinetics analysis for crystallization kinetics of non-crystallization solid, Journal of Non-Crystalline Solids 320 (1–3) (2003) 84–91.

[26] Y.J. Park, J. Heo, Nucleation and crystallization kinetics of glass derived from incinerator fly ash waste, Ceramics International 28 (6) (2002) 669–673.

[27] T.K. Mukhopadhyay, S. Ghatak, H.S. Maiti, Pyrophyllite as raw material for ceramic applications in the perspective of its pyro-chemical properties, Ceramics International 36 (2010) 909–916.

[28] O.P. Filho, G.P.L. Torre, L.L. Hench, Effect of crystallization on apatite-layer formation of bioactive glass 45S5, Journal of Biomedical Materials Research 30 (4) (1996) 509–514.

[29] C. Huang, E.C. Behrman, Structure and Properties of Calcium Aluminosilicate Glasses, Journal of Non-Crystalline Solids 128 (1991) 310–321.

[30] E.Y. Guseva, M.N. Gulyukin, Effect of fluoride additives on formation in the SiO_2–CaO–Al_2O_3 System, Inorganic Materials 38 (2002) 962–965.

[31] C.I. Merzbacher, W.B. White, The structure of alkaline earth aluminosilicate glasses as determined by vibrational spectroscopy, Journal of Non-Crystalline Solids 130 (1) (1991) 18–34.

[32] K. Ramaswamy, M. Kamalakkan, Infrared study of some south Indian clays, Indian Journal of Pure and Applied Physics 25 (4) (1987) 284–286.

[33] S. Bhattacharyya, S. Ghatak, Synthesis and characterization of YAG precursor powder in the hydroxyhydrogel form, Ceramics International 35 (1) (2009) 29–34.

[34] M. Zhu, B. Wang, P. Liu, H. Yan, Z. Ding, Preparation and properties of $BaTiSi_2O_7$ glass-ceramics, Optical Materials 23 (1–2) (2003) 323–326.

[35] K. Ikeda, H. Kinoshita, R. Kawamura, A. Yoshikawa, O. Kobori, A. Hiratsuka, Production of high-strength glass-ceramics from industrial wastes using phase equilibrium diagram of CaO–Al_2O_3–SiO_2 system, Journal of Solid Mechanics and Materials Engineering 5 (5) (2011) 209–218.